FITTING OF LATERAL RESISTANCES IN SILICON SOLAR CELLS TO ELECTROLUMINESCENCE IMAGES

D. Kiliani[1], A. Herguth[1], G.Hahn[1], V. Rutka[2], M. Junk[2]
University of Konstanz, [1]Department of Physics / [2]Department of Mathematics and Statistics,
78457 Konstanz, Germany

ABSTRACT: A technique for fast quantitative determination of the different terms contributing to series resistance in a solar cell from electroluminescence (EL) is introduced. A two-dimensional model of the solar cell is presented, which is used to fit the measured luminescence intensities and thereby separate the series resistance contributions of fingers and emitter. First quantitative results of this method for an industrial screen printed monocrystalline silicon solar cell are shown and the influence of lateral diffusion of charge carriers on the measurement is discussed.
Keywords: Electrical Properties, Electroluminescence, Modelling

1 INTRODUCTION

In the past few years, luminescence imaging methods have become popular for wafer and solar cell characterization. The recorded images provide information about a variety of cell parameters, as published in previous papers [1].

One prominient feature in EL images is the lateral change of luminescence intensity caused by series resistances [2]. At excitation current densities near J_{SC} of the cell these lateral resistances in fingers and emitter lead to a noticeable reduction of the local diode voltage. The voltage drop increases with increasing distance the current has to take through finger and emitter. This leads to the reduced luminescence intensity that can be seen in the center between fingers and between busbars, e.g. in the EL measurement displayed in Fig. 1.

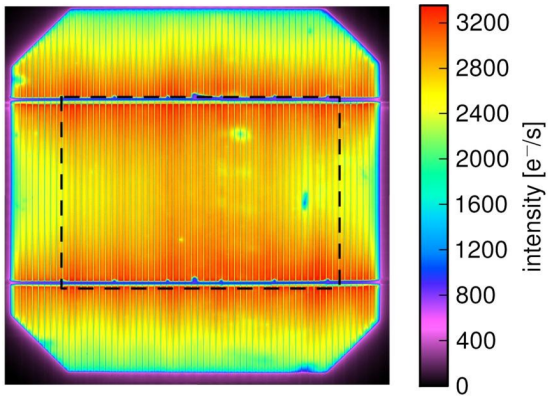

Figure 1: Electroluminescence image of a mono-crystalline 12.5×12.5 cm² silicon solar cell under an excitation current density of 30 mA/cm². The black rectangle marks the area used in the averaging process (see section 3).

2 MATHEMATICAL MODEL

To separate the various parameters which have an effect on the local p-n junction voltage, a multilayered model of the solar cell was developed. It includes lateral resistances in the metallization and the emitter layer and yields a voltage distribution of the cell surface, which can be fitted to the EL measurements.

2.1 Description of the model

In Fig. 2 the schematic layout of a solar cell with screen printed front metallization is shown. The figure shows the series resistances (blue, green, yellow) that were included in the mathematical model of the solar cell. The local diode characteristics (red) were simulated by the two-diode model:

$$J(U) = -J_{ph} + J_{01}\left(\exp\left(\frac{eU}{k_B T}\right) - 1\right) + J_{02}\left(\exp\left(\frac{eU}{2k_B T}\right) - 1\right) + \frac{U}{R_{sh}}$$

The modeled area shown in Fig. 2 is determined by the symmetry constraints in a solar cell. The whole area of a screen printed silicon solar cell is a periodic repetition of the area between the fingers, provided the voltage along the busbars is constant. In a homogeneous solar cell the voltage profile along each finger can therefore be assumed to be the same, which leads to two kinds of symmetry axes parallel to the fingers: One in the middle of each finger (Γ_F) and one in the middle between two fingers (Γ_S). Correspondingly, the symmetry axes parallel to the busbars lie on the busbar and in the middle between busbars (Γ_B and Γ_S).

The whole area of a homogeneous solar cell can therefore be modeled by regarding the area between two symmetry axes, resulting in a symmetry reduced area with a width of half the finger distance and a height of half the busbar distance.

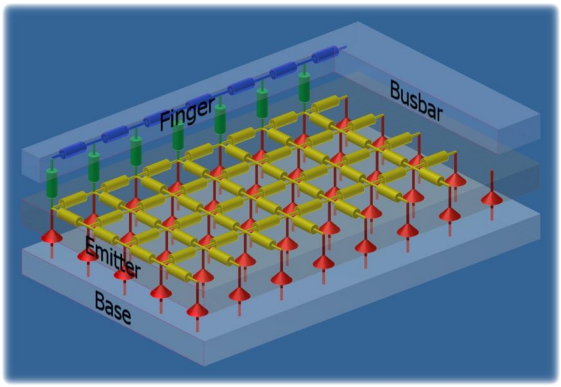

Figure 2: Schematic layout of the solar cell model. The resistances are depicted in a discrete grid only for this illustration, the mathematical model uses continuous conductance values.

2.2 Formulation of the model

In contrast to the simplified depiction in Fig. 2, the mathematical model is continuous along the two lateral dimensions. The current flow in the emitter area Ω, along with the currents flowing into and out of it lead to a second order differential equation $\Sigma_E \Delta U = -J(U_{ext} - U)$, where Σ_E is the emitter conductance, U is the voltage relative to the busbar, U_{ext} is the voltage between busbar and back contact and J is the current density of the two-diode model. The boundary conditions can be expressed as

$$U = 0 \quad \text{on } \Gamma_B$$
$$U = \overline{U}_E \text{ on } \Gamma_F$$
$$n \cdot \nabla U = 0 \quad \text{on } \Gamma_S$$

where $\overline{U}_E$ is the average voltage of the emitter under the finger area, n is the normal vector of the respective border and $\Gamma_{B,F,S}$ are the busbar-, finger- and symmetry-borders, respectively.

The voltage in the contact fingers $\overline{U}_C$ and the coupling between emitter and metallization is described by the following set of equations:

$$\Sigma_E \overline{U}_E'' + \frac{1}{\Delta_F} \Sigma_E \left.\frac{\partial U}{\partial y}\right|_{\Gamma_F} = \overline{K} - \overline{J}_E \text{ on } \Gamma_F$$
$$\Sigma_F \overline{U}_C'' = -\overline{K} \quad \text{on } \Gamma_F$$
$$\overline{J}_E = J(U_{ext} - \overline{U}_E; J_{ph} = 0)$$
$$\overline{K} = \frac{1}{R_C}(\overline{U}_E - \overline{U}_C)$$

Here, y is the direction perpendicular to the finger and Σ_F is the finger conductance. The boundary conditions in the finger are $\overline{U}_C(\Gamma_B) = \overline{U}_E(\Gamma_B) = 0$ and $\overline{U}'_C(\Gamma_S) = \overline{U}'_E(\Gamma_S) = 0$.

The complete system of nonlinear partial differential equations was solved using a second order accurate finite difference discretization, combined with Newton's method.

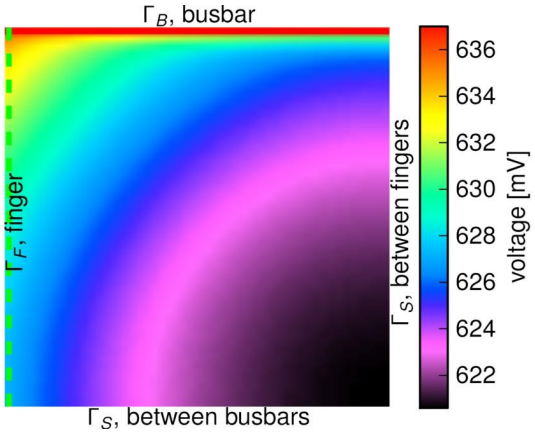

Figure 3: Solution of the p-n junction voltage distribution. Model parameters were $R_{finger} = 300$ mΩ/cm, $R_{emitter} = 50$ Ω/sq, $R_{contact} = 3$ mΩcm², $U_{ext} = 637$ mV. The displayed area is 1 mm wide and 30 mm high and represents the symmetry region.

3 FITTING PROCEDURE

3.1 Symmetry reduced EL images

To compare the mathematical solar cell model with the measured image data, the EL images have to be reduced to the same symmetry region the model describes. This requires the exact positions of the busbars and fingers in the EL image to be known. An algorithm to automatically detect busbars and fingers was developed, based on autocorrelation of the EL image.

To rule out edge effects, only the center area of the solar cell was used (see black rectangle in Fig. 1). The intensity data of each symmetry region in this area was averaged and yields the distribution shown in Fig. 4. Because the aspect ratio of the symmetry region of about 1:30 is inapt for display, the plot is streched to a square geometry.

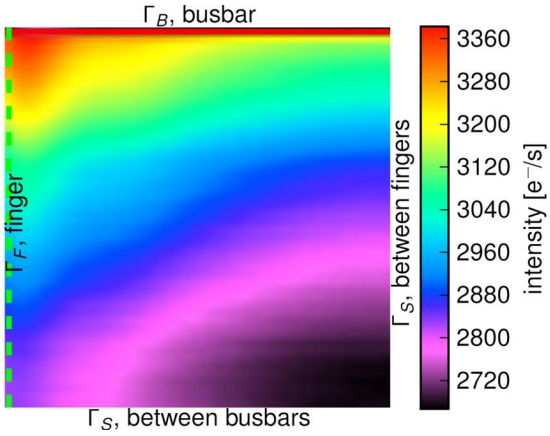

Figure 4: Average of the EL image shown in Fig. 1, reduced to the area between symmetry axes as described in section 2.

3.2 Intensity – voltage conversion

To convert the measured luminescence intensities to p-n junction voltages, the rate of spontaneous photon emission is used [3]:

$$R_{sp}(E_\gamma) = \frac{\alpha(E_\gamma) E_\gamma^2}{4\pi^2 \hbar^3 c^2} \frac{1}{\exp\left(\frac{E_\gamma - \Delta\eta}{k_B T}\right) - 1} \quad \text{(eq. 1)}$$

This emission rate depends on the energy of the emitted photon E_γ, the absorption coefficient α and the speed of light c. Assuming a homogeneous diffusion length [4], the integral luminescence intensity over all wavelengths only depends on the second term of eq. 1.

As the exponential term is very large under EL measurement conditions, the -1 term can be neglected. The p-n junction voltage, which corresponds to the quasi fermi niveau splitting Δη, is then determined by the logarithm of the luminescence intensity. Any prefactors in the above equation result in an additive constant to the junction voltage. Using the externally measured voltage as a reference and comparing it with the maximum of the voltages from EL yields a distribution of absolute p-n junction voltages.

3.3 Determination of the model parameters

The mathematical model was then fitted to the solar cell using a least squares approximation of the voltage distribution from the model and the voltage distribution calculated from the EL measurement. The finger line

resistance, contact resistance and emitter sheet resistance were fitted, while the diode parameters and parallel resistance were kept fixed at the values previously determined from IV measurement. As the mathematical model does not account for the missing EL emission from areas covered by the metallization, the left and upper borders of the symmetry region, where the fingers and busbars are located, were excluded from the fit error calculation.

3.4 Fit results

The presented fitting procedure was applied to the EL measurement shown in Fig. 1. For comparison, the resistance values were determined with traditional methods. The emitter sheet resistance of the cell is 50 Ω/sq, the line resistance of the fingers was determined to 325 mΩ/cm with a 4-point measurement of the resistance between the busbars. The contact resistance between metallization and emitter could not be measured nondestructively, it probably lies in the range of 1–10 mΩcm².

The fitting algorithm returned values of 10.1 Ω/sq for the emitter sheet resistance, 127 mΩ/cm for the finger line resistance and consistently ran into the imposed optimization constraint of 0.1 mΩcm² for the contact resistance.

To discover the source of these discrepancies, the voltage along the fingers was measured under the same excitation conditions as the EL image (30 mA/cm²). The measured voltages are shown in Fig. 5, along with the values on the left edge of the voltage distribution from EL.

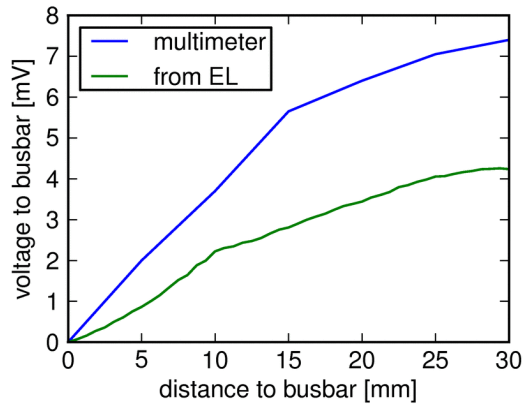

Figure 5: Voltage drop along the finger relative to the busbar potential.

The measurements differ significantly by a factor of about 1.75, which could not be explained by any term in equation 1. When the voltage gradient of the measured EL voltage distribution was amplified by this factor, the finger line resistance was fitted to 320 mΩ/cm and the emitter sheet resistance to 24.4 Ω/sq.

Both the still unsatisfactory sheet resistance result and the qualitatively different voltage distributions from EL and from the mathematical model suggest that the error can not be caused by a linear effect which affects both dimensions to the same degree.

The lateral diffusion of excited minority carriers in the base of the solar cell was investigated as a potential cause of the reduced voltage contrast. While this diffusion current could not yet be integrated into the model, it will obviously lead to a reduced contrast in the EL image. To simulate the effect, a Gaussian filter was applied to the modeled voltage distribution (see Fig. 3). The standard deviation σ of the gauss distribution was set to 0.5 mm for best fit to the measured voltage map, the result is shown in Fig. 6. It shows much better accordance to the measured distribution shown in Fig. 4.

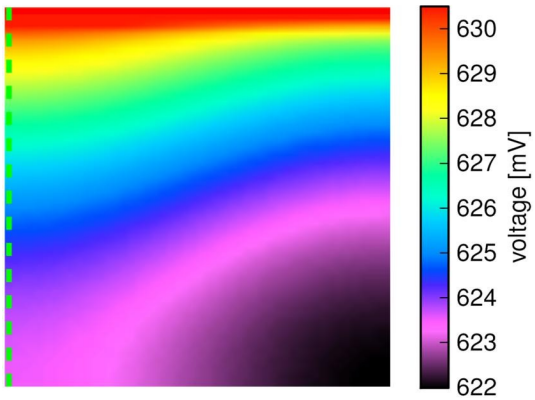

Figure 6: Voltage distribution from model after a Gaussian filter with σ = 0.5 mm was applied to simulate electron diffusion in the solar cell base.

4 CONCLUSION

The presented method allows for a fast, quantitative and nondestructive measurement of series resistances in crystalline silicon solar cells. First results show a promising qualitative agreement between measurements and simulation. While the lateral diffusion of charge carriers was not yet included into the solar cell model, a simulation of its effects on the voltage distribution leads to an even better reproduction of the voltage maps generated from electroluminescence images.

The lateral diffusion can also explain the observed reduction of image contrast, which leads to systematically too low series resistance values when fitting the solar cell model to EL measurements. A big improvement of quantitative values obtained by the fitting procedure can be expected when carrier diffusion is accounted for in the mathematical model.

This work was supported by funding of the German BMU under contract number 0325033.

5 REFERENCES

[1] M. Kasemann et al., Proc. 23rd EUPVSEC, p. 965 (2008)

[2] T. Trupke, E. Pink, R.A. Bardos and M.D. Abbott, Appl. Phys. Lett. 90, p. 202102 (2007)

[3] P. Würfel, Physics of Solar Cells, Wiley-VCH (2005)

[4] P. Würfel, T. Trupke, T. Puzzer, E. Schaeffer, W. Warta and S.W. Glunz, J. Appl. Phys. 101, p. 123110 (2007)